Chemical Science

ROYAL SOCIETY OF CHEMISTRY

EDGE ARTICLE

View Article Online
View Journal | View Issue

Cite this: *Chem. Sci.*, 2025, **16**, 3130

All publication charges for this article have been paid for by the Royal Society of Chemistry

Received 17th December 2024
Accepted 6th January 2025

DOI: 10.1039/d4sc08530b

rsc.li/chemical-science

Thiosemicarbazones as versatile photoswitches with light-controllable supramolecular activity†

Bengi Sentürk,[a] Burkhard Butschke [b] and Fabian Eisenreich *[a]

Using photoswitchable molecules to manipulate supramolecular interactions under light illumination has driven advancements in numerous fields, allowing for the strategic alteration of molecular systems. However, integrating the moiety responsible for these interactions into the photochromic scaffold can be complex and may hamper the switching efficiency. We thus explored a simple class of organic molecules, namely thiosemicarbazones, featuring both a photoisomerizable C=N double bond and a thiourea moiety capable of hydrogen bonding. The scalable two-step synthesis allowed us to prepare 23 thiosemicarbazones to systematically elucidate their optical properties. Attaching various functional groups, extended π-systems, and heterocycles enabled fine-tuning of their absorption profiles. UV light illumination converts thiosemicarbazones from the stable *E*-isomer to the metastable *Z*-isomer, exhibiting both negative and positive T-type photochromism, a wide range of thermal half-lives, PSS values up to 92%, and high fatigue resistance. Substituting the C=N moiety with a pyridinyl group stabilizes the *Z*-isomer *via* intramolecular hydrogen bonding, confirmed by single-crystal X-ray analysis, and transforms thiosemicarbazones into bistable P-type photoswitches. Additionally, thiosemicarbazones dimerize or form aggregates through hydrogen bonding—a process that can be turned off or on with light. Overall, thiosemicarbazones offer tunable photochromic and supramolecular properties, rendering them a promising photoswitch for creating stimuli-responsive systems.

Introduction

Photoswitches refer to molecules capable of undergoing reversible conversion from one state, or isomer, to another upon exposure to light of a certain wavelength.[1] The switching process has the potential to cause a substantial geometric shift through isomerization around a double bond, as demonstrated in stiff-stilbene,[2,3] (hemi)indigo,[4–6] azobenzene,[7–10] and diazocine systems.[11,12] This transformative event can be strategically harnessed to exert control over the interplay of molecules, in particular *via* supramolecular interactions.[13–15] A notable degree of precision has been achieved in steering ion transport,[16] supramolecular assemblies,[17–24] non-equilibrium systems,[25–27] photopharmacology,[28,29] and catalysis,[30–32] among various other functions, with light. Photoswitches thus prove instrumental for breaking the static boundaries of chemical processes and infusing them with newfound adaptability.

Yet, tethering the moiety accountable for the non-covalent interactions to the photochromic scaffold may entail elaborate synthesis procedures[33] and impair the switching performance relative to the standalone photoswitch.[27] From the viewpoint of molecular design, rendering the supramolecular unit an integral component of the photoswitch structure-rather than attaching it later on-would simplify the process. This led us to explore thiosemicarbazones (TSCs), an organic compound class formally consisting of a thiourea unit linked to a C=N double bond, whose photoswitching capabilities are yet to be fully unveiled (Fig. 1). On the one hand, thiourea groups are widely recognized as versatile hydrogen bonding partners. On the other hand, photoswitches featuring C=N double bonds have attracted considerable attention as potential alternatives to

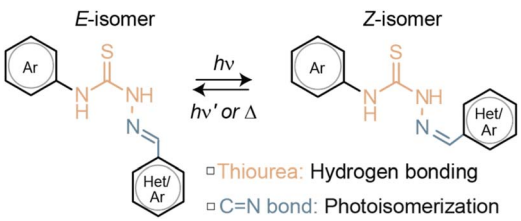

Fig. 1 Photoisomerization of thiosemicarbazones.

[a]*Department of Chemical Engineering and Chemistry, Institute for Complex Molecular Systems, Eindhoven University of Technology, 5600 MB, Eindhoven, The Netherlands. E-mail: f.r.eisenreich@tue.nl*

[b]*Institute for Inorganic and Analytical Chemistry, University of Freiburg, Albertstr. 21, 79104 Freiburg, Germany*

† Electronic supplementary information (ESI) available: Materials and methods, experimental procedures, NMR spectroscopy, single-crystal X-ray diffraction, UV/vis spectra, PSS determination, quantum yield, dimerization constant determination studies, light-induced aggregation, additional references. CCDC 2358067, 2358068, 2358069, 2358070, 2358071, 2358072 and 2358493. For ESI and crystallographic data in CIF or other electronic format see DOI: https://doi.org/10.1039/d4sc08530b

traditional olefin or azo analogs, owing to their comparable or even superior properties.[34–37] They offer distinct advantages, such as tunable properties, high photoconversion efficiency, ease of derivatization, and scalability in synthesis.

Hydrazones, extensively studied by Aprahamian *et al.*, are one notable member of this photoswitch class.[38] Besides their facile synthesis and high photostationary states (PSS), hydrazones demonstrate bistability, exhibiting photochromism in both directions (P-type) along with remarkable thermal stability of the metastable isomer lasting up to thousands of years. Additionally, some hydrazone derivatives can exhibit very short thermal half-lives, leading to T-type behavior in specific cases.[39,40] Hecht *et al.* introduced acylhydrazones as another versatile photoswitch class within this category.[41] In addition to displaying the desired photoswitch properties seen in hydrazones, acylhydrazones also present a range of thermal stabilities for their *Z*-isomer, ranging from short-lived to thermally stable derivatives. By suitable substitution, acylhydrazones display not only P-type but also T-type photochromism, wherein back-isomerization occurs *via* the ground state rather than the excited state. Unlike (acyl) hydrazones, the thiourea moiety in TSCs provides a strong binding motif for supramolecular interactions that may be adjustable with light. However, the photochromic properties of TSCs remain largely unexplored. Scattered reports exist in literature, in which light-induced proton transfer[42–44] as well as $E \rightarrow Z$ isomerization of a single compound,[45] both in the solid state, are described. Instead, thiosemicarbazones are primarily acknowledged for their biochemical activity (*e.g.*, antibacterial, antifungal, and antitumor)[46,47] as well as their coordination affinity to a broad range of metal ions.[48]

In this work, we comprehensively explore the photochromic properties of TSCs and introduce them as a promising class of photoswitches. The simple yet high-yielding synthesis allowed us to prepare a library of TSCs, including 23 compounds, and systematically investigate their structure–property relationships. In-depth optical and NMR spectroscopy measurements demonstrate the pronounced tuneability of the photoisomerization around the C=N double bond. The library not only encompasses T-type photoswitches, featuring thermal half-lives of the metastable *Z*-isomer ranging from minutes to hours, along with stable *Z*-isomers, but also P-type photoswitches exhibiting photoisomerization in both switching directions. Moreover, the *E*-isomer of TSCs tends to form weakly associated dimers through hydrogen bonds in solution. The generation of the *Z*-isomer completely shuts down this interaction by sterically shielding the thiourea group, thereby providing the means to toggle between assembled and disassembled states on-demand with light. Overall, the easily accessible synthesis of TSCs, combined with their diverse photochromic properties and adjustable supramolecular interactions, positions them as a promising newcomer to the photoswitch family.

Results and discussion

Synthesis and molecular design

Thiosemicarbazones can be readily prepared in two simple synthetic steps with excellent yields and straight-forward purification. First, an aromatic isothiocyanate derivative was treated with hydrazine monohydrate in dry CH_2Cl_2 at 0 °C to yield the corresponding thiosemicarbazide within 30 min (Fig. 2A, see the ESI† for details). The condensation of the thiosemicarbazide with an aromatic carbonyl compound in ethanol and the presence of trace amounts of trifluoroacetic acid as a catalyst resulted in the formation of the final thiosemicarbazone. After both reaction steps, the products conveniently precipitated from the mixtures. Consequently, a simple filtration and washing process is all that was required to obtain highly pure molecules. A diverse range of thiosemicarbazides is also commercially available, which generally simplifies the synthesis further. To demonstrate the feasibility of the synthesis protocol, we performed the reactions on a gram-scale (Fig. 2A, right). Based on this rapid and efficient synthesis, we prepared a library of 23 differently substituted TSCs to explore structure–property relationships (Fig. 2B). The as-synthesized TSCs remained stable and showed no signs of hydrolysis of the C=N double bond for at least one year, both in the solid state and when dissolved in $CDCl_3$ and DMSO-d_6. The compounds were ambiguously characterized using variety of analytical methods (*i.e.*, ^{1}H, ^{13}C, and ^{19}F NMR spectroscopy, FT-IR spectroscopy, and mass spectrometry; Fig. S1–S58 in the ESI†).

Our molecular design process was driven by the following considerations: **TSC-1** with phenyl groups attached to both the thiourea and C=N double bond serves as the reference compound. In *para*-position of the N-phenyl group, we introduced $-NO_2$ (**TSC-2**) and –CN (**TSC-3**) as electron-withdrawing (EW) groups as well as –OMe (**TSC-4**) and $-NMe_2$ (**TSC-5**) as electron-donating (ED) groups. **TSC-6** features two trifluoromethyl substituents positioned *meta* to the thiourea, as $-CF_3$ groups hold a privileged position not only in drug and catalyst design (*e.g.*, Schreiner's catalyst), but also in enhancing the fatigue resistance of photoswitches.[49] We applied the same *para*-substitution pattern to the C-phenyl moiety (**TSC-7**–**TSC-10**) and incorporated various halides (**TSC-11**–**TSC-14**). The latter was motivated by the potential of *ortho*-halogenation in azobenzene to generate photoswitches with long-lived *Z*-isomers and near-quantitative PSS.[50–52] The C=N moiety was further functionalized with various extended π-systems (**TSC-15**–**TSC-17**) to shift the absorption profile of the TSCs towards the visible region of the electromagnetic spectrum. Lastly, we investigated heterocyclic derivatives (**TSC-18**–**TSC-23**), as heterocycles are commonly found in molecular photoswitches and can be crucial to their function.[6,7,49]

To gain deeper insight into the molecular geometry of TSCs, we analysed their molecular structure by single-crystal X-ray diffraction. Single crystals were obtained at room temperature by slow solvent evaporation. All analysed TSCs exhibited a *trans–cis* conformation on their thiourea core, corroborated by 2D NMR analysis (Fig. S59 in the ESI†). **TSC-1**, **TSC-4**, **TSC-13**, **TSC-14**, **TSC-19**, and **TSC-20** crystallized in the *E*-configuration, while **TSC-22** adopted the *Z*-configuration (Fig. S60–S66 in the ESI†). Analysis of **TSC-22** indicated the presence of an intramolecular H-bond between the thiourea and pyridinyl functionalities (N–H···N: 1.990 Å) examination of the X-ray data also revealed the rotational freedom of the N-phenyl group, which exhibits dihedral angles in the range from 8° to 98°. In contrast,

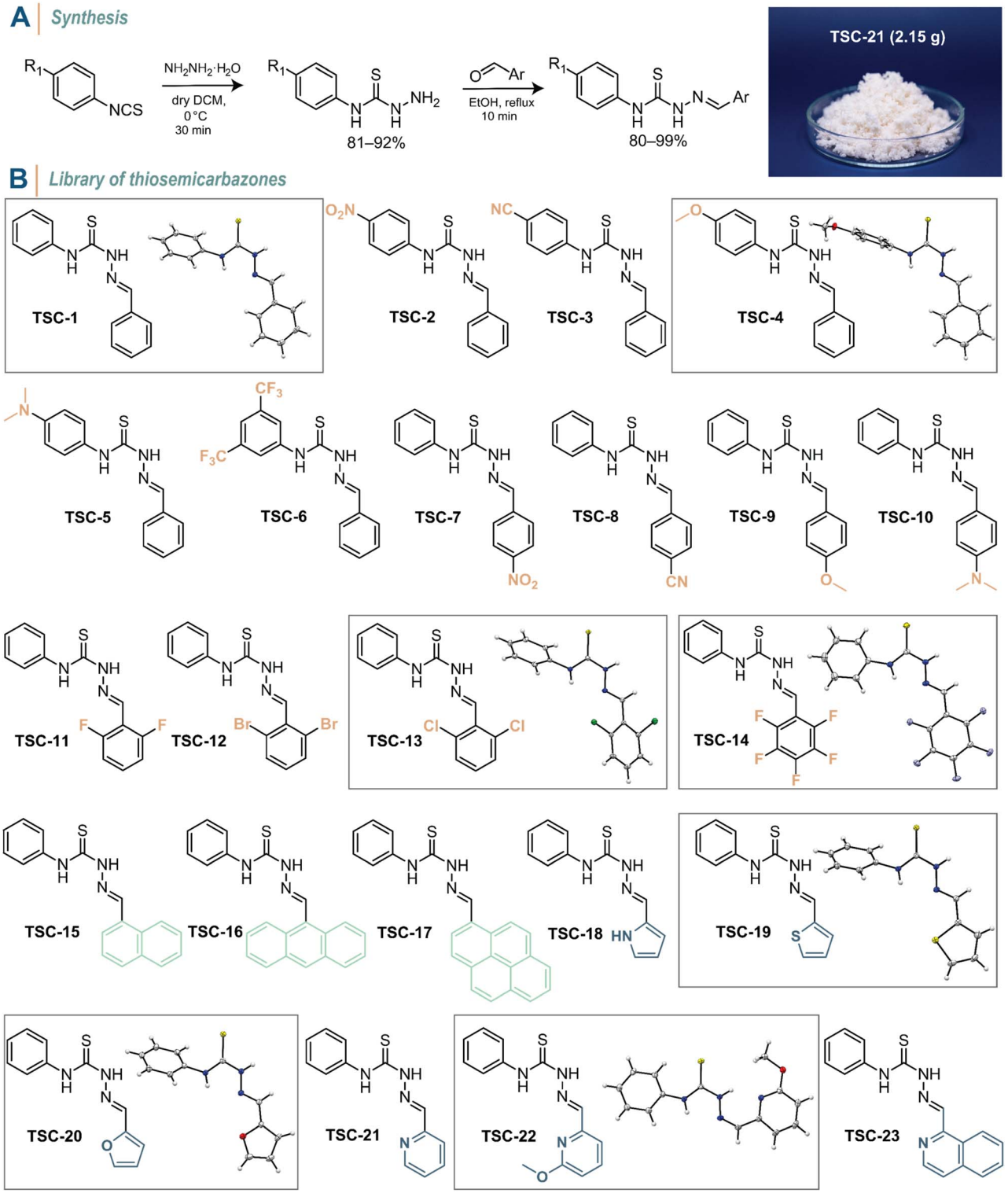

Fig. 2 Library of TSCs. (A) General two-step synthesis scheme to prepare functionalized TSCs. A photograph of compound **TSC-21** showcases the scalability of the synthesis. (B) Chemical structures of all synthesized TSCs. Single-crystal X-ray structures of **TSC-1**, **TSC-13**, **TSC-14**, **TSC-19**, **TSC-20**, and **TSC-22** are depicted with thermal ellipsoids representing 50% probability (40% and 17% disorders of the furanyl and thienyl rings, respectively, have been omitted for clarity). C: grey, H: off-white, N: blue, S: yellow, O: red, Cl: green, and F: purple.

the C-phenyl group is oriented in the same plane as the C=N and thiourea moieties unless a bulky substituent such as chlorine is incorporated, causing deviation from planarity by up to 35°. The detailed structural information obtained from single-crystal X-ray diffraction provided a foundational understanding of the molecular geometry of TSCs.

Optical properties of TSC-1

To explore the behaviour of thiosemicarbazones under light illumination, we first conducted UV-vis spectroscopy studies on **TSC-1** in an acetonitrile solution ($c = 3.8 \times 10^{-5}$ M, 20 °C, Fig. 3A, S67–S69 in the ESI†). The dissolved compound showed an absorption maximum in the UV region ($\lambda_{max} = 319$ nm) and

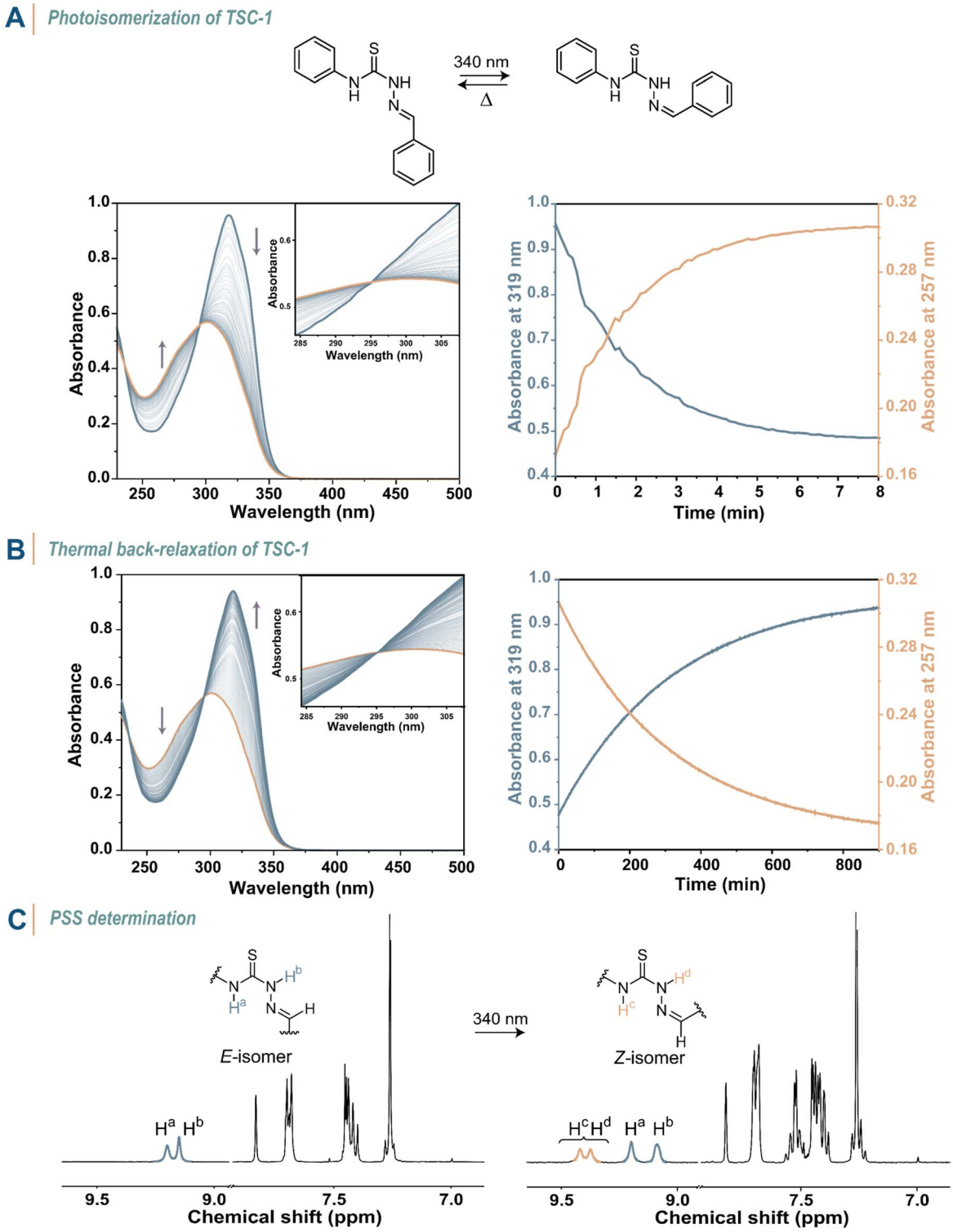

Fig. 3 Photoisomerization studies on **TSC-1**. (A) Conversion of **TSC-1**$_E$ (blue line) in MeCN ($c = 3.77 \times 10^{-5}$ M) to **TSC-1**$_{PSS}$ (orange line) under constant light irradiation ($\lambda_{irr} = 340$ nm) followed over time (left) and absorbance at $\lambda = 319$ nm and 257 nm followed over time (right). (B) Thermal back-relaxation of **TSC-1**$_{PSS}$ (left) and absorbance at $\lambda = 319$ nm and 257 nm followed over time (right). (C) ^{1}H NMR spectra (400 MHz, 25 °C, $CDCl_3$) of **TSC-1**$_E$ before and after illumination with 340 nm until reaching the PSS of 44%.

Table 1 Quantitative comparison of TSCs

Photoswitch	$\varepsilon(E)$ [M^{-1} cm^{-1}]	$\lambda_{max}(E)$ [nm]	λ_{max}(PSS)[a] [nm]	$\Delta\lambda_{max}$[b] [nm]	$t_{1/2}$[c]	$E:Z$ ratio at PSS (λ_{irr})
TSC-1	35 400	319	302	−17	199 min	56 : 44 (365 nm)[d]
TSC-2	39 700	328	321	−7	32 min	n.d.
TSC-3	39 000	321	304	−17	1.35 min	n.d.
TSC-4	35 000	317	307	−10	20 min	n.d.
TSC-5	37 200	316	312	−4	118 min	n.d.
TSC-6	33 100	321	318	−3	1 min	n.d.
TSC-7	28 300	361	351	−10	258 min	33 : 67 (365 nm)[e]
TSC-8	32 500	337	328	−9	213 min	53 : 47 (365 nm)[e]
TSC-9	35 200	328	317	−11	37 min	n.d.
TSC-10	47 500	367	437	70	11 min	n.d.
TSC-11	35 200	318	293	−25	10.7 h	24 : 76 (365 nm)[e]
TSC-12	21 300	309	284	−25	1 day	10 : 90 (365 nm)[e]
TSC-13	23 400	314	283	−31	Stable	8 : 92 (365 nm)[e]
TSC-14	37 600	318	293	−25	53 min	25 : 75 (365 nm)[e]
TSC-15	28 800	349	276	−73	76 min	18 : 82 (365 nm)[e]
TSC-16	12 800	389	364	−25	Stable	59 : 41 (365 nm)[e]
TSC-17	41 600	406	405	−1	66 min	n.d.
TSC-18	31 900	338	402	64	6 min	n.d.
TSC-19	31 300	337	407	70	46 min	n.d.
TSC-20	37 200	328	323	−5	Stable	22 : 78 (365 nm)[d]
TSC-21	n.d.	320[f]	325	5	Stable	82 : 18 (405 nm)[d]
						67 : 33 (340 nm)[d]
TSC-22	n.d.	333[f]	355	22	Stable	85 : 15 (365 nm)[d]
						36 : 64 (340 nm)[d]
TSC-23	n.d.	340[f]	376	36	192 min	22 : 78 (365 nm)[d]

[a] Defined as the most red-shifted absorption band. [b] Defined as $\Delta\lambda_{max} = \lambda_{max}(PSS) - \lambda_{max}(E)$. [c] Measured at 20 °C; photoswitches were labeled as thermally stable when no thermal $Z \rightarrow E$ isomerization was observed for at least 60 min.[41] [d] Determined based on ^{1}H NMR experiments in MeCN-d_3 *via* LED illumination. [e] Determined based on ^{1}H NMR experiments in $CDCl_3$ *via* LED illumination. In cases of short-lived *Z*-isomers, the PSS was not determined. [f] λ_{max} for dark equilibrium state.

a high extinction coefficient at this wavelength (ε = 35 400 M^{-1} cm^{-1}, Table 1). Upon irradiation with an LED (λ_{irr} = 340 nm), the absorption at the absorption maximum decreased and a new absorption band at 302 nm built up, until reaching the PSS. Due to this hypsochromic shift ($\Delta\lambda_{max} = -17$ nm), **TSC-1** classifies as a negative photochrome. The clear isosbestic point at 295 nm suggests a clean conversion from **TSC-1$_E$** to **TSC-1$_Z$** upon irradiation. Complete back-isomerization to the thermodynamically stable *E*-isomer occurred thermally over time after the light source was turned off (Fig. 3B). The thermal half-life of the metastable *Z*-isomer was determined as $t_{1/2}$ = 199 min. Illumination with light of other wavelengths did not induce back-isomerization, thus **TSC-1** demonstrates pure T-type photoswitch behaviour. We further quantified the composition of both isomers at the PSS with ^{1}H NMR spectroscopy, showing 44% of *Z*-isomer in the equilibrium state (Fig. 3C).

We then carried out a solvent screening study to assess if there is a correlation between polarity or hydrogen bonding ability of the solvent and the photoswitching performance of **TSC-1** (Fig. S70–S74 in the ESI†). In highly polar solvents (*e.g.*, DMF, DMSO) and protic media (*e.g.*, MeOH, EtOH) barely any spectral changes were observed under UV light illumination, presumably because these solvents stabilize the *E*-isomer through hydrogen bonding,[53] leading to rapid thermal back-isomerization of the *Z*-isomer. In contrast, **TSC-1** responded well to light in less polar and aprotic solvents. For instance, the thermal half-lives observed in EtOAc and THF were measured at $t_{1/2}$ = 66 and 83 min, respectively. Solvents with low hydrogen bonding capability, such as $CHCl_3$, toluene, and acetonitrile, yielded a prolonged thermal stability of the *Z*-isomer with $t_{1/2}$ = 120, 181, and 199 min, respectively. While a detailed mechanistic study is required to fully understand these effects, the observed trends are summarized in Table S2 of the ESI.†

To investigate the influence of sulfur on the optical properties of thiosemicarbazones, we compared **TSC-1** with its oxygen analog, semicarbazone **SC-1** (Fig. S75 in the ESI†). From the absorption profile in acetonitrile, it is apparent that **SC-1** requires higher energy light for photoisomerization (λ_{max} = 293 nm) and has a lower molar absorption coefficient at the absorption maximum (ε = 25 000 M^{-1} cm^{-1}) compared to **TSC-1**. These findings suggest that sulfur enhances light absorption efficiency and reduces the energy required for activation, making it advantageous for photoswitch design. This is consistent with studies demonstrating that the steric size of sulfur elongates the C=X bond, which results in an energy drop of the $\pi^*_{C|S}$ relative to $\pi^*_{C|O}$, thereby reducing the HOMO–LUMO gap.[54,55]

Interestingly, the steric repulsion of sulfur also increases the electronegativity of the C=X bond, despite sulfur being the more electropositive chalcogen atom.[56] This is supported by NMR spectroscopy, which shows a downfield shift of the N–H proton signals (Fig. S76 in the ESI†).

Photoswitching studies on TSC library

Satisfied with the pronounced photoisomerization of **TSC-1**, we continued with analyzing the optical properties of the other TSC compounds in acetonitrile solutions (Fig. S77–S115 in the ESI†). Aside from the molar extinction coefficients of the *E*-isomers ranging from 12 800 to 47 500 M^{-1} cm^{-1} at their λ_{max} (Table 1), the key discoveries are summarized as follows. Anchoring EW and ED groups in *para*-position of the N-phenyl group had only marginal effect on the λ_{max} values of the *E*-isomers of **TSC-2**–**TSC-5**, while the $t_{1/2}$ values of the *Z*-isomers generally shortened. **TSC-6** with two $-CF_3$ groups in *meta*-position showed the lowest $t_{1/2}$ of 1 min among all library members. The stability of the *Z*-isomer of these photoswitches shows no apparent correlation with EW or ED groups. This is likely due to the rotational flexibility of the N-phenyl group around the C–N bond and its considerable distance from the C=N bond, which make electronic effects difficult to evaluate. Substituting the *para*-position of the C-phenyl moiety (**TSC-7**–**TSC-10**) resulted, however, in a clear trend, as ED groups decrease and EW groups increase the thermal half-lives of the *Z*-isomers relative to the parent **TSC-1**. Interestingly, the absorption maxima of **TSC-7**–**TSC-9** shifted hypsochromically upon UV light illumination with $\Delta\lambda_{max}$ in the range of −9 to −11 nm, while **TSC-10** functionalized with $-NMe_2$ revealed a new absorption band in the visible region at 437 nm ($\Delta\lambda_{max}$ = 70 nm). **TSC-10** thus classifies as a positive photochrome, with the benefit of distinct absorption band separation. Next in line, we studied the *ortho*-halogenated chromophores and observed a significant elevation in the thermal stability of their *Z*-isomers. While **TSC-11** and **TSC-12** feature fluorides and bromides, respectively, with half-lives of 10.7 h and 1 day, **TSC-13** containing chlorides demonstrates bistability, at least under the operating conditions. **TSC-14** bearing a pentafluorophenyl group, however, showed a significantly shorter half-life of 53 min, highlighting the exclusive role of *ortho*-halogens in stabilizing the *Z*-isomers. This trend is also evident in azobenzenes, indicating that *ortho*-halogenation contributes to the prolonged thermal stability of the *Z*-isomer.[50–52] Furthermore, the high photoconversion yields observed in **TSC-11**–**TSC-14** compared to other TSCs can be attributed to the greater separation between the π–π* spectral bands of the *E*- and *Z*-isomers, which facilitates a more selective and efficient light absorption of the *E*-isomer at the irradiation wavelength (Fig. S95–S101 in the ESI†).[57] While **TSC-11** and **TSC-14** show partial overlap between these bands, resulting in PSS values of approximately 75%, **TSC-12** and **TSC-13** achieve exceptional PSS values of ≥90% (Fig. S116–S124 in the ESI†). By extending the π-conjugation through larger aromatic moieties, such as transitioning from phenyl to naphthyl (**TSC-15**), anthracenyl (**TSC-16**), and pyrenyl (**TSC-17**), the λ_{max} of the *E*-isomers expectedly shifted towards the blue edge of the visible spectrum. To verify that anthracene does not form dimers as a side reaction under light irradiation, we exposed a $CDCl_3$ solution of **TSC-16** to 365 nm light and analyzed it using ^1H NMR spectroscopy (Fig. S123 in the ESI†). No signals were detected around 4.5 ppm, which would indicate anthracene dimerization.[58] Instead, the results confirmed the successful formation of 41% *Z*-isomer at the PSS.

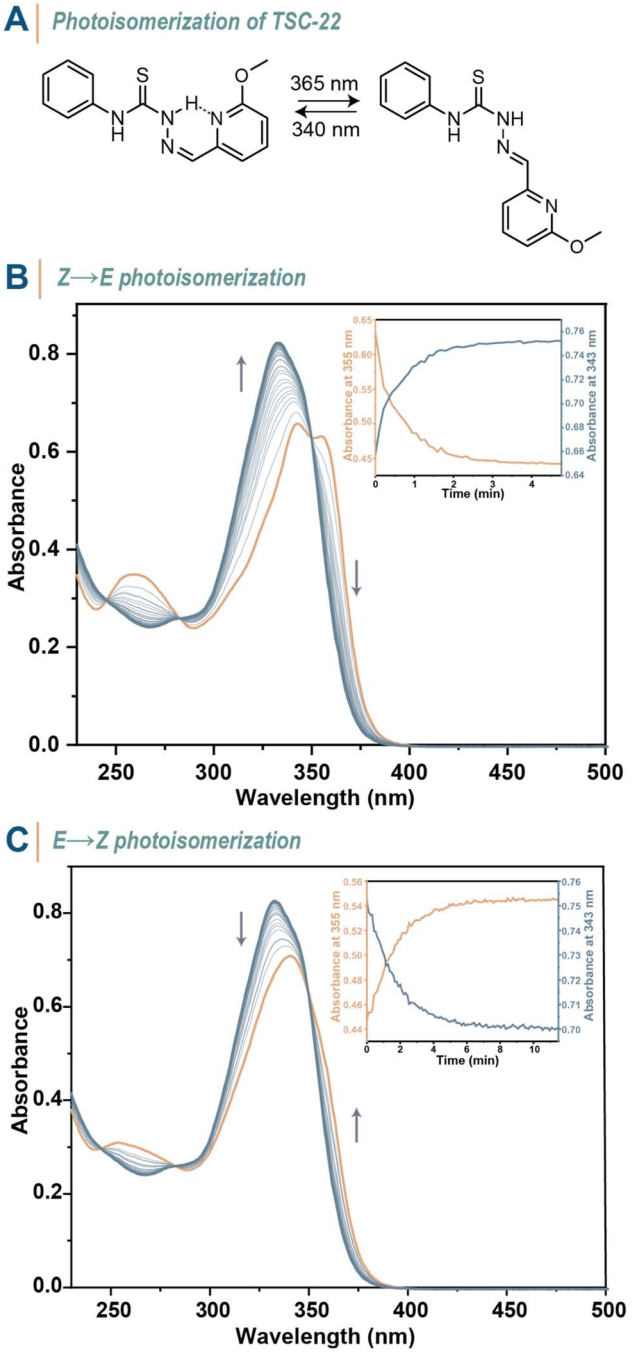

Fig. 4 (A) Bidirectional photoisomerization of **TSC-22**. (B) Conversion of **TSC-22** (orange line) in MeCN ($c = 2.68 \times 10^{-5}$ M) to $\textbf{TSC-22}_{PSS}$ (blue line) followed over time under constant irradiation (λ_{irr} = 365 nm). (C) Conversion of $\textbf{TSC-22}_{PSS}$ (blue line) to **TSC-22** (orange line) followed over time under constant irradiation (λ_{irr} = 340 nm). The insets show changes in absorbance at 343 and 355 nm followed over time during illumination.

Lastly, heterocyclic TSCs were explored, revealing a significant impact on the photoswitching performance. Similar to **TSC-10**, both pyrrolyl **TSC-18** and thienyl **TSC-19** demonstrate positive photochromism, characterized by a new red-shifted absorption band emerging at approximately 405 nm.[41] The new absorption band observed in **TSC-10**, **TSC-18**, and **TSC-19**

may be attributed to an intramolecular hydrogen transfer occurring in the excited state, forming a tautomeric species. Similar behaviour has been reported for acylhydrazones,[41] where theoretical calculations indicate that the *Z*-tautomer formed *via* intramolecular hydrogen transfer leads to a red shift in the absorption spectrum.[59] This spectral feature was absent in furanyl **TSC-20**. Instead, the *Z*-isomer of **TSC-20** displayed remarkable thermal stability, likely due to the presence of an intramolecular hydrogen bond between the thiourea N–H and the oxygen atom on the furan ring.

Intrigued by this finding, we anticipated a comparable stabilization of the *Z*-isomer in pyridinyl derivatives **TSC-21**–**TSC-23**. To explore this further, we first conducted a thorough analysis on **TSC-21** using both UV-vis and NMR spectroscopy techniques. Illuminating a solution of **TSC-21** with blue light ($\lambda_{irr} = 405$ nm) resulted in the formation of a thermally stable equilibrium state, similar to furanyl **TSC-20**. However, ^{1}H NMR measurements unveiled that the initial mixture of **TSC-21** in MeCN-d_3 was composed of an almost equal $E:Z$ ratio of 47 : 53 (Fig. S125 in the ESI†). This composition can be attributed to pyridine's stronger propensity as a hydrogen bond acceptor compared to furan. Upon exposure to blue light, the $E:Z$ ratio converted to 82 : 18. More importantly, when the solution was then illuminated with 340 nm, the $E:Z$ ratio slightly adjusted to 67 : 33. This observation marks the first evidence of P-type photochromism in TSCs. To enhance the stability of the *Z*-isomer even further, we introduced an electron-donating –OMe group in **TSC-22** (Fig. 4A). Due to the boost in electron density around the nitrogen atom of the pyridinyl group, **TSC-22** showed an enriched initial $E:Z$ ratio of 2 : 98 in MeCN-d_3 (Fig. S126 in the ESI†). The intramolecular H-bond and the presence of a pseudo six-membered aromatic ring contribute to the stability of **TSC-21**$_Z$, as evidenced by its single-crystal X-ray structure. Photoisomerization ($\lambda_{irr} = 365$ nm) to the energetically less preferred *E*-isomer led to a thermally stable PSS (Fig. 4B), which was comprised of a $E:Z$ ratio of 85 : 15. Subsequent back-isomerization with 340 nm light yielded an $E:Z$ ratio of 36 : 64, consistent with the spectral changes observed in UV-vis spectroscopy (Fig. 4C).

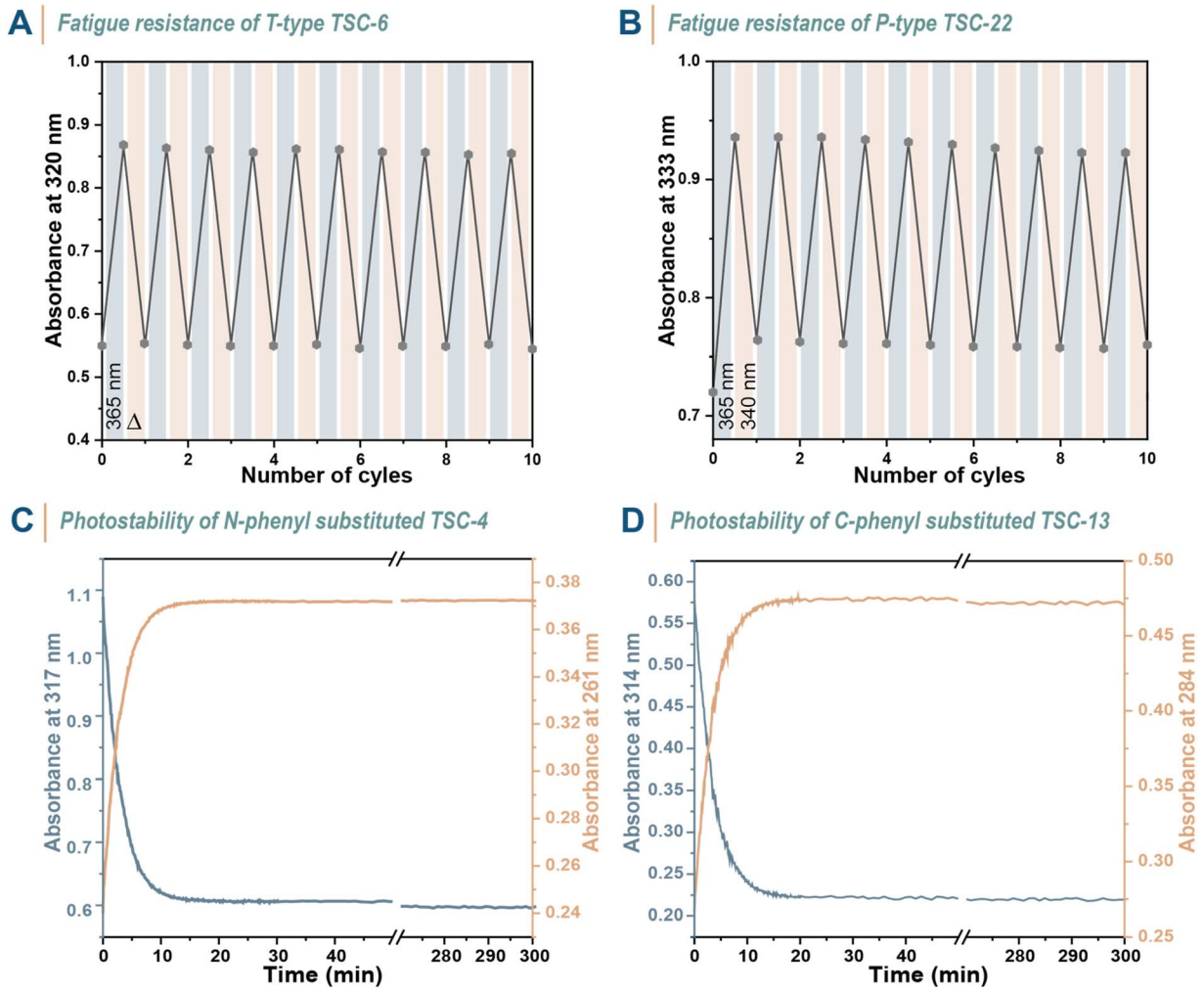

Fig. 5 Photostability of TSCs. (A) Change in absorbance at $\lambda_{max}(E)$ during photoswitching cycles of **TSC-6** in MeCN ($c = 2.90 \times 10^{-5}$ M) based on alternating irradiation with 365 nm LED until reaching the PSS and complete thermal back-relaxation. (B) Change in absorbance at $\lambda_{max}(E)$ during photoswitching cycles of **TSC-22** in MeCN ($c = 2.68 \times 10^{-5}$ M) based on alternating irradiation with 365 and 340 nm LEDs until reaching the PSS in both directions. (C) Long-term irradiation of **TSC-4** in MeCN ($c = 3 \times 10^{-5}$ M) and (D) of **TSC-13** in MeCN ($c = 3.14 \times 10^{-5}$ M).

Lastly, we were interested in the potential impact of an electron-deficient quinolinyl moiety on the photoswitching behaviour. As anticipated, ^{1}H NMR analysis revealed that the initial mixture of **TSC-23** in MeCN-d_3 was composed of an $E:Z$ ratio of 78 : 22 due to a weaker intramolecular hydrogen bond. Upon 365 nm light exposure, the $E:Z$ ratio flipped to 22 : 78 (Fig. S127 in the ESI†). Interestingly, it was not possible to back-isomerize **TSC-23**$_Z$ with light. Instead this isomer thermally relaxed to the initial composition over time with $t_{1/2} = 192$ min. This underlines the crucial role of electron-rich pyridinyl groups in rendering TSCs bistable P-type photoswitches.

To maximize the utility of photoswitches, they should undergo photoisomerization with minimal fatigue over numerous switching cycles. Hence, we explored the light stability of several compounds. **TSC-6** was selected as a fast-relaxing T-type photoswitch and subjected to repetitive photoisomerization with 365 nm light until reaching the PSS and then allowed to relax back thermally before initiating the next cycle (Fig. 5A). A similar experiment was performed on **TSC-22**, only with the difference that back-isomerization was induced using 340 nm light instead of thermal energy (Fig. 5B). Both chromophores demonstrated stability, showing no significant signs of fatigue over at least 10 switching cycles. Prolonged UV light irradiation for 5 h did also not induce a spectral change that indicate light-induced degradation, as evidenced by UV-vis spectroscopy experiments on **TSC-4** and **TSC-13** (Fig. 5C and D). These experiments highlight the reliability of thiosemicarbazones as photoswitches.

To further evaluate the efficiency of the photoisomerization, quantum yields were determined for selected compounds at 365 nm. The halogenated TSCs were chosen due to their high thermal half-lives, with the following values: **TSC-11** ($\Phi_{E\rightarrow Z} = 0.85$), **TSC-12** ($\Phi_{E\rightarrow Z} = 0.33$), **TSC-13** ($\Phi_{E\rightarrow Z} = 0.58$), and **TSC-14** ($\Phi_{E\rightarrow Z} = 0.83$, Table S3 and Fig. S128 in the ESI†). These values are comparable or superior to those of (acyl)hydrazone photoswitches.[41,60]

Supramolecular properties

After investigating the structure–property relationship of thiosemicarbazones in terms of their photoswitching capability, we were inspired by the potential of modulating the supramolecular interactions between these molecules in solution using light. First, we assessed whether the *E*-isomer of

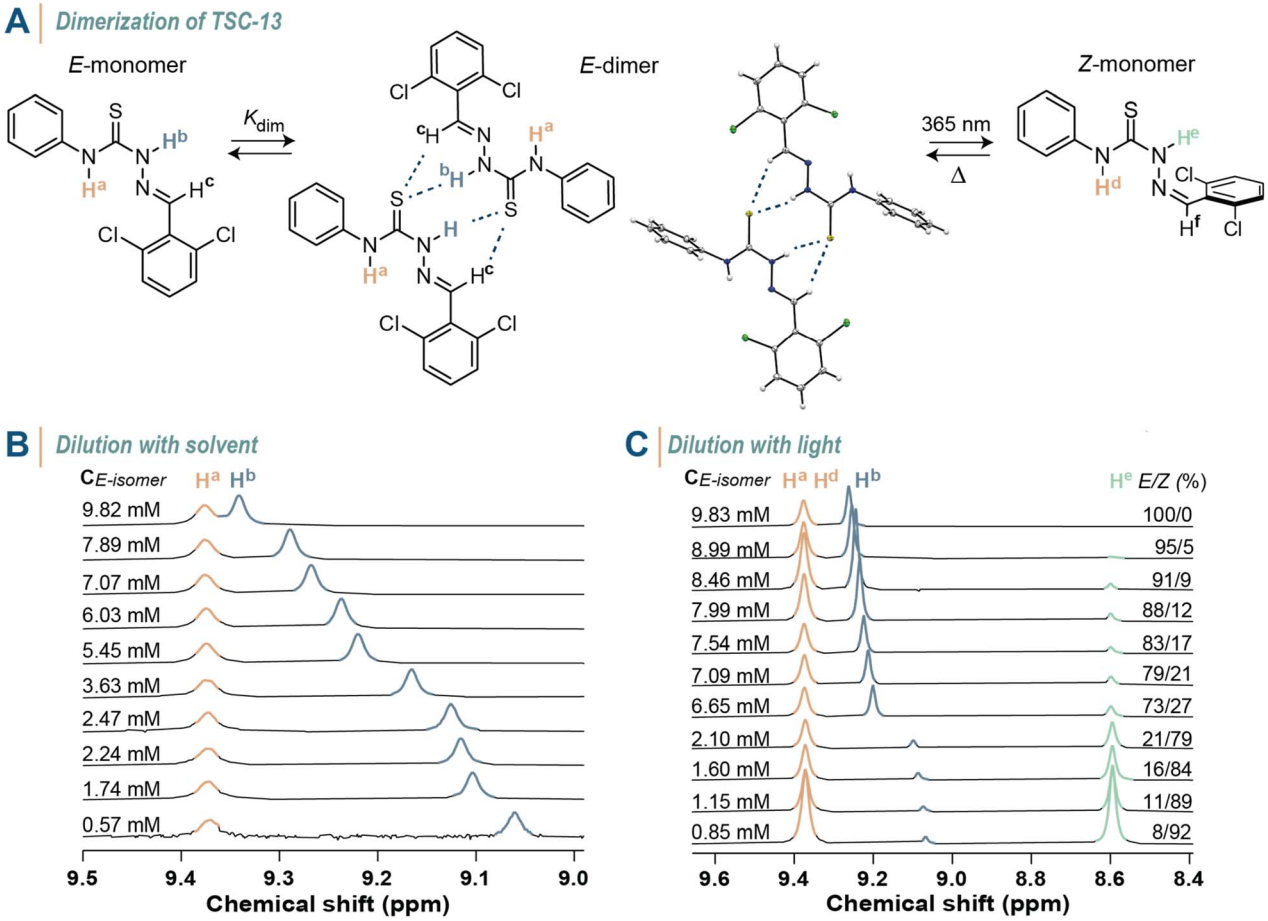

Fig. 6 Light-controlled supramolecular interactions. (A) Dimerization of **TSC-13**$_E$ through H-bonding (as confirmed by single-crystal X-ray analysis), which can be turned off when switched to **TSC-13**$_Z$. (B) ^{1}H NMR spectra (400 MHz, 25 °C, $CDCl_3$) of **TSC-13** solutions with varying concentrations. (C) ^{1}H NMR spectra (400 MHz, 25 °C, $CDCl_3$) at various stages of irradiation with 365 nm highlighting the emergence of new signals attributed to **TSC-13**$_Z$.

thiosemicarbazones dimerizes in solution through hydrogen bonding between the sulfur atom of the thiourea group and hydrogen atoms H^b and H^c, as the single crystal structure analysis of **TSC-13** suggests (Fig. 6A). When switching to the *Z*-isomer, this interaction is anticipated to be completely turned off by steric shielding of the binding site, thereby providing the opportunity to toggle between dimeric and monomeric states. We thus selected **TSC-13$_E$** as a model compound due to its pronounced thermal stability and prepared a series of solutions with concentrations ranging from 9.82 to 0.57 mM in $CDCl_3$. In ^{1}H NMR spectra we observed a characteristic shift in the H^b and H^c signals towards high field as the concentration decreased (Fig. 6B and S129 in the ESI†). The chemical shift of H^a remained constant, as this proton is not directly involved in the dimerization process. Correlating the shift in H^b signal with the varying concentration allowed us to determine the binding constant which was obtained from two analyses with minimal standard deviation, yielding $K_{dim} = 6.44 \pm 0.01\ M^{-1}$. Instead of adjusting the concentration of **TSC-13$_E$** to determine its binding affinity—which is experimentally more elaborate—we also explored the option of 'diluting' the photoswitch in solution with light. We thus irradiated a $CDCl_3$ solution containing **TSC-13$_E$** (c = 9.83 mM) with 365 nm light and recorded ^{1}H NMR spectra at various stages of the process (Fig. 6C and S130 in the ESI†). Through photoisomerization we gradually reduced the quantity of binding **TSC-13$_E$** in solution and thus effectively diluted the compound with respect to the constant volume of solvent. Accordingly, we observed a consistent trend in the chemical shift of the H^b and H^c signals of **TSC-13$_E$**, which yielded a comparable dimerization constant of $6.18 \pm 0.34\ M^{-1}$. At the same time, we confirmed that the formed **TSC-13$_Z$** did not participate in binding events due to steric constraints, since the new signals assigned to **TSC-13$_Z$**, such as H^e at 8.6 ppm, remained constant throughout the experiment. The same experiments were conducted on **TSC-11** yielding comparable values (Fig. S131 and S132 in the ESI†). These findings showcase that the non-covalent interactions between thiosemicarbazones can be turned off at will by means of light.

Motivated to enhance the supramolecular interactions among thiosemicarbazones, we examined the behaviour of pyridine-substituted **TSC-21** in a concentrated toluene solution. While the *Z*-isomer is inherently more stable in an apolar solvent due to intramolecular hydrogen bonds, we anticipated that photoisomerization to the *E*-isomer would unleash both binding sites—the thiourea and pyridine moiety—resulting in the formation of larger supramolecular aggregates (Fig. 7). When we exposed **TSC-21** solution with an initial $E:Z$ ratio of 20 : 80 to 365 nm light, we observed that 91% of the photoswitch precipitated from the solution. To recover the initial state, we simply heated the mixture, facilitating the back-isomerization to the soluble *Z*-isomer. A subsequent cycle of light-induced precipitation and heat-induced dissolution demonstrated the reproducibility of the process with the same $E:Z$ ratio maintained and 90% of the *E*-isomer precipitated (Fig. S133 in the ESI†). To further study the aggregation behaviour, we performed SEM analysis on the precipitate, which forms a more complex morphology compared to **TSC-21** obtained from toluene prior to light illumination (Fig. S134 in the ESI†).

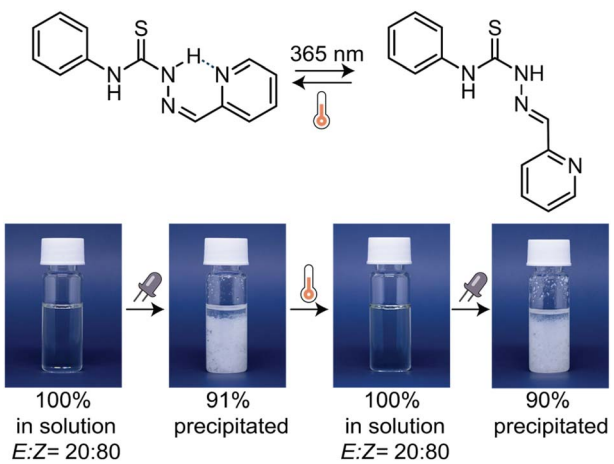

Fig. 7 Photographs showing two cycles of the light-induced aggregation and precipitation of TSC-21 from a 15 mM solution in toluene with 365 nm LED, followed by the heat-induced dissolution due to thermal back-relaxation.

Conclusions

This comprehensive study demonstrates the photoisomerization capabilities of thiosemicarbazones and their light-responsive supramolecular interactions. By systematically decorating thiosemicarbazones with various substituents, we uncovered a broad spectrum of characteristics, encompassing shifts in absorption maxima spanning 91 nm, PSS values reaching 92%, negative and positive photochromism, alongside T- and P-type photoswitching. The thermal stability of the less stable isomer showed tunability, with thermal half-lives ranging from as short as 1 min to as long as 1 day, and some remaining stable within the timeframe of observation. Additionally, thiosemicarbazones display dimerization or aggregation facilitated by intermolecular hydrogen bonding, which can be (de)activated by light on demand. This wide range of features combined with its ease of synthesis renders thiosemicarbazones an attractive and versatile newcomer in the photoswitch family. Given their potential biological activity and notable binding affinity to metal ions, thiosemicarbazones could find promising application in photopharmacology[61,62] or light-controlled recognition of charged species.[63] Relatively weak supramolecular interactions, as showcased in this study, have also shown to be essential in substrate activation,[64,65] thereby suggesting tunable catalysis as another potential research direction. Overall, these findings pave the way for designing and developing novel light-responsive molecular systems with precisely adjustable functionalities.

Data availability

The X-ray crystallographic coordinates for structures reported in this study have been deposited at the Cambridge Crystallographic Data Centre (CCDC) under deposition numbers

2358493 (**TSC-1**), 2358067 (**TSC-4**), 2358068 (**TSC-13**), 2358069 (**TSC-14**), 2358070 (**TSC-19**), 2358071 (**TSC-20**), and 2358072 (**TSC-22**).† Copies of the data can be obtained free of charge *via* **https://www.ccdc.cam.ac.uk/structures/**. All other data supplementary the findings of this study, including experimental procedures and compound characterization, NMR spectroscopy, single-crystal X-ray diffraction, UV/vis spectroscopy, are available within the article and its ESI.† All data are available from the corresponding author upon request.

Author contributions

B. S. conducted syntheses, performed UV/vis and NMR spectroscopy experiments, analysed and interpreted data. B. B. solved the single crystal X-ray structures. B. S. and F. E. conceived the idea, designed the study, and wrote the manuscript. All authors discussed the results and edited the manuscript.

Conflicts of interest

There are no conflicts to declare.

Acknowledgements

We are grateful to Prof. Željko Tomović for fruitful scientific discussions and acknowledge Luc Rijnders for his contributions to the synthesis of TSCs. We also thank Dr Christos Pantazidis for the SEM analyses and Roegaya Sabera for the photographs. F.E. acknowledges the financial support by the Dutch Research Council NWO (VENI grant no. VI.Veni.212.215).

Notes and references

1 A. Goulet-Hanssens, F. Eisenreich and S. Hecht, *Adv. Mater.*, 2020, **32**, 1905966.
2 D. Villarón and S. J. Wezenberg, *Angew. Chem., Int. Ed.*, 2020, **59**, 13192–13202.
3 F. Xu, J. Sheng, C. N. Stindt, S. Crespi, W. Danowski, M. F. Hilbers, W. J. Buma and B. L. Feringa, *Chem. Sci.*, 2024, **15**, 6763–6769.
4 K. Kuntze, J. Viljakka, M. Virkki, C. Y. Huang, S. Hecht and A. Priimagi, *Chem. Sci.*, 2023, **14**, 2482–2488.
5 C. Y. Huang and S. Hecht, *Chem.–Eur. J.*, 2023, **29**, e202300981.
6 V. Josef, F. Hampel, H. Dube, V. Josef, F. Hampel and H. Dube Friedrich-Alexander, *Angew. Chem., Int. Ed.*, 2022, **61**, 202210855–202210856.
7 S. Crespi, N. A. Simeth and B. König, *Nat. Rev. Chem.*, 2019, **3**, 133–146.
8 J. Gemen, J. R. Church, T.-P. Ruoko, N. Durandin, M. J. Białek, M. Weißenfels, M. Feller, M. Kazes, M. Odaybat, V. A. Borin, R. Kalepu, Y. Diskin-Posner, D. Oron, M. J. Fuchter, A. Priimagi, I. Schapiro and R. Klajn, *Nat. Rev. Chem.*, 2019, **3**, 133–146.
9 J. Isokuortti, K. Kuntze, M. Virkki, Z. Ahmed, E. Vuorimaa-Laukkanen, M. A. Filatov, A. Turshatov, T. Laaksonen, A. Priimagi and N. A. Durandin, *Chem. Sci.*, 2021, **12**, 7504–7509.
10 S. A. M. Steinmüller, M. Odaybat, G. Galli, D. Prischich, M. J. Fuchter and M. Decker, *Chem. Sci.*, 2024, **15**, 5360–5367.
11 H. Lee, J. Tessarolo, D. Langbehn, A. Baksi, R. Herges and G. H. Clever, *J. Am. Chem. Soc.*, 2022, **144**, 3099–3105.
12 J. Ewert, L. Heintze, M. Jordà-Redondo, J. S. Von Glasenapp, S. Nonell, G. Bucher, C. Peifer and R. Herges, *J. Am. Chem. Soc.*, 2022, **144**, 15059–15071.
13 Z. Yang, Z. Liu and L. Yuan, *Asian J. Org. Chem.*, 2021, **10**, 74–90.
14 F. Xu and B. L. Feringa, *Adv. Mater.*, 2023, **35**, 2204413.
15 E. Nieland, J. Voss and B. M. Schmidt, *Synlett*, 2022, **34**, 975–982.
16 S. J. Wezenberg, L. J. Chen, J. E. Bos, B. L. Feringa, E. N. W. Howe, X. Wu, M. A. Siegler and P. A. Gale, *J. Am. Chem. Soc.*, 2022, **144**, 331–338.
17 J. de Jong, M. A. Siegler and S. J. Wezenberg, *Angew. Chem., Int. Ed.*, 2024, **63**, e202316628.
18 G. Tyagi, J. L. Greenfield, B. E. Jones, W. N. Sharratt, K. Khan, D. Seddon, L. A. Malone, N. Cowieson, R. C. Evans, M. J. Fuchter and J. T. Cabral, *JACS Au*, 2022, **2**, 2670–2677.
19 D. Hugenbusch, M. Lehr, J. S. von Glasenapp, A. J. McConnell and R. Herges, *Angew. Chem., Int. Ed.*, 2023, **62**, e202212571.
20 E. Nieland, J. Voss and B. M. Schmidt, *ChemPlusChem*, 2023, **88**, e202300353.
21 E. Weyandt, G. M. Ter Huurne, G. Vantomme, A. J. Markvoort, A. R. A. Palmans and E. W. Meijer, *J. Am. Chem. Soc.*, 2020, **142**, 6295–6303.
22 L. Wei, S. T. Han, T. T. Jin, T. G. Zhan, L. J. Liu, J. Cui and K. Da Zhang, *Chem. Sci.*, 2021, **12**, 1762–1771.
23 R. G. Dinardi, A. O. Douglas, R. Tian, J. R. Price, M. Tajik, W. A. Donald and J. E. Beves, *Angew. Chem., Int. Ed.*, 2022, **61**, e202205701.
24 A. D. W. Kennedy, R. G. Dinardi, L. L. Fillbrook, W. A. Donald and J. E. Beves, *Angew. Chem., Int. Ed.*, 2022, **61**, e202205701.
25 M. Canton, J. Groppi, L. Casimiro, S. Corra, M. Baroncini, S. Silvi and A. Credi, *J. Am. Chem. Soc.*, 2021, **143**, 10890–10894.
26 M. Kathan, S. Crespi, N. O. Thiel, D. L. Stares, D. Morsa, J. de Boer, G. Pacella, T. van den Enk, P. Kobauri, G. Portale, C. A. Schalley and B. L. Feringa, *Nat. Nanotechnol.*, 2022, **17**, 159–165.
27 J. J. B. van der Tol, T. A. P. Engels, R. Cardinaels, G. Vantomme, E. W. Meijer and F. Eisenreich, *Adv. Funct. Mater.*, 2023, **33**, 202301246.
28 P. Kobauri, F. J. Dekker, W. Szymanski and B. L. Feringa, *Angew. Chem., Int. Ed.*, 2023, **62**, e202300681.
29 K. Hüll, J. Morstein and D. Trauner, *Chem. Rev.*, 2018, **118**, 10710–10747.
30 K. Grill and H. Dube, *J. Am. Chem. Soc.*, 2020, **142**, 19300–19307.
31 G. C. Thaggard, J. Haimerl, R. A. Fischer, K. C. Park and N. B. Shustova, *Angew. Chem., Int. Ed.*, 2023, **62**, e202302859.

32 Q. Qiu, Z. Sun, D. Joubran, X. Li, J. Wan, K. Schmidt-Rohr and G. G. D. Han, *Angew. Chem., Int. Ed.*, 2023, **62**, e202300723.
33 B. Tang, M. Pauls, C. Bannwarth and S. Hecht, *J. Am. Chem. Soc.*, 2024, **146**, 45–50.
34 L. Greb, G. Vantomme and J. M. Lehn, in *Molecular Photoswitches: Chemistry, Properties, and Applications, 2 Volume Set*, Wiley-VCH Verlag, 2022, vol. 1–2, pp. 325–349.
35 J. Wu, L. Kreimendahl, S. Tao, O. Anhalt and J. L. Greenfield, *Chem. Sci.*, 2024, **15**, 3872–3878.
36 L. D. Thai, T. R. Guimaraes, L. C. Chambers, J. A. Kammerer, D. Golberg, H. Mutlu and C. Barner-Kowollik, *J. Am. Chem. Soc.*, 2023, **145**, 14748–14755.
37 D. Veselý, J. Jančík, M. Weiter, D. Blasi, N. Ivanova, J. Krajčovič and A. Georgiev, *J. Photochem. Photobiol., A*, 2022, **430**, 113994.
38 B. Shao and I. Aprahamian, *Chem*, 2020, **6**, 2162–2173.
39 Q. Li, H. Qian, B. Shao, R. P. Hughes and I. Aprahamian, *J. Am. Chem. Soc.*, 2018, **140**, 11829–11835.
40 H. Qian, S. Pramanik and I. Aprahamian, *J. Am. Chem. Soc.*, 2017, **139**, 9140–9143.
41 D. J. Van Dijken, P. Kovaříček, S. P. Ihrig and S. Hecht, *J. Am. Chem. Soc.*, 2015, **137**, 14982–14991.
42 Y. Che, L. Liu, Y. Tang, Y. Qiao, X. Zhao, S. Gao, S. Ding and D. Jia, *New J. Chem.*, 2017, **41**, 15229–15235.
43 J. Hu, L. Liu, D. Jia, J. Guo, X. Xie, D. Wu and R. Sheng, *J. Photochem. Photobiol., A*, 2011, **217**, 117–124.
44 X. Xie, L. Liu, D. Jia, J. Guo, D. Wu and X. Xie, *New J. Chem.*, 2009, **33**, 2232–2240.
45 Y. Che, L. Liu, J. Zhao, Y. Yu and X. Zhao, *Dyes Pigm.*, 2019, **169**, 105–110.
46 Y. Tsai, N. Aira, D. Ensinck, C. Banchio, H. Gramajo, A. G. Suárez, R. A. Spanevello and A. M. Sarotti, *ChemistrySelect*, 2023, **8**, e202303776.
47 E. Palma, P. Raposinho, M. P. C. Campello, D. Belo, J. F. Guerreiro, V. Alves, A. Fonseca, A. J. Abrunhosa, A. Paulo and F. Mendes, *Eur. J. Inorg. Chem.*, 2021, **2021**, 1337–1348.
48 A. I. Matesanz, A. B. Caballero, C. Lorenzo, A. Espargaró, R. Sabaté, A. G. Quiroga and P. Gamez, *Inorg. Chem.*, 2020, **59**, 6978–6987.
49 M. Herder, B. M. Schmidt, L. Grubert, M. Pätzel, J. Schwarz and S. Hecht, *J. Am. Chem. Soc.*, 2015, **137**, 2738–2747.
50 L. N. Lameijer, S. Budzak, N. A. Simeth, M. J. Hansen, B. L. Feringa, D. Jacquemin and W. Szymanski, *Angew. Chem., Int. Ed.*, 2020, **59**, 21663–21670.
51 K. Hema, A. B. Grommet, M. J. Białek, J. Wang, L. Schneider, C. Drechsler, O. Yanshyna, Y. Diskin-Posner, G. H. Clever and R. Klajn, *J. Am. Chem. Soc.*, 2023, 24755–24764.
52 D. Bléger, J. Schwarz, A. M. Brouwer and S. Hecht, *J. Am. Chem. Soc.*, 2012, **134**, 20597–20600.
53 C. Laurence, S. Mansour, D. Vuluga, A. Planchat and J. Legros, *J. Org. Chem.*, 2021, **86**, 4143–4158.
54 C. Nieuwland and C. Fonseca Guerra, *Chem.–Eur. J.*, 2024, **30**, e202304361.
55 Y. L. Wu and A. I. Wright, *Phys. Chem. Chem. Phys.*, 2023, **25**, 1342–1348.
56 C. Nieuwland, R. Verdijk, C. Fonseca Guerra and F. M. Bickelhaupt, *Chem.–Eur. J.*, 2024, **30**, e202304161.
57 R. Lin, P. K. Hashim, S. Sahu, A. S. Amrutha, N. M. Cheruthu, S. Thazhathethil, K. Takahashi, T. Nakamura, T. Kikukawa and N. Tamaoki, *J. Am. Chem. Soc.*, 2023, **145**, 9072–9080.
58 G. W. Breton and X. Vang, *J. Chem. Educ.*, 1998, **75**, 81.
59 M. Moreno, R. Gelabert and J. M. Lluch, *Phys. Chem. Chem. Phys.*, 2019, **21**, 16075–16082.
60 B. Shao, H. Qian, Q. Li and I. Aprahamian, *J. Am. Chem. Soc.*, 2020, **141**, 8364–8371.
61 S. Samanta, A. A. Beharry, O. Sadovski, T. M. McCormick, A. Babalhavaeji, V. Tropepe and G. A. Woolley, *J. Am. Chem. Soc.*, 2013, **135**, 9777–9784.
62 M. J. Fuchter, *J. Am. Chem. Soc.*, 2020, **63**, 11436–11447.
63 M. Natali and S. Giordani, *Chem. Soc. Rev.*, 2012, **41**, 4010–4029.
64 D. Larsen, L. M. Langhorn, O. M. Akselsen, B. E. Nielsen and M. Pittelkow, *Chem. Sci.*, 2017, **8**, 7978–7982.
65 C. Thomas, F. Peruch, A. Deffieux, A. Milet, J. P. Desvergne and B. Bibal, *Adv. Synth. Catal.*, 2011, **353**, 1049–1054.